Impact of substrate induced band tail states on the electronic and optical properties of MoS_2

J. Klein,[1,2,*] A. Kerelsky,[3] M. Lorke,[4,5] M. Florian,[4] F. Sigger,[1] J. Kiemle,[1] M. C. Reuter,[6] T. Taniguchi,[7] K. Watanabe,[7] J. J. Finley,[1,2,8] A. Pasupathy,[3] A. W. Holleitner,[1,2,8] F. M. Ross,[6,9,†] and U. Wurstbauer[2,10,‡]

[1] *Walter Schottky Institut and Physik Department, Technische Universität München, 85748 Garching, Germany*

[2] *Nanosystems Initiative Munich (NIM), 80799 Munich, Germany*

[3] *Department of Physics, Columbia University, New York, New York 10027, United States*

[4] *Institut für Theoretische Physik, Universität Bremen, 28334 Bremen, Germany*

[5] *Bremen Center for Computational Materials Science, University of Bremen, 28359 Bremen, Germany*

[6] *IBM T. J. Watson Research Center, Yorktown Heights, NY 10598, United States*

[7] *National Institute for Materials Science, Tsukuba, Ibaraki 305-0044, Japan*

[8] *Munich Center for Quantum Science and Technology (MCQST), 80799 Munich, Germany*

[9] *Department of Materials Science and Engineering, Massachusetts Institute of Technology, Cambridge, MA 02139, United States*

[10] *Institute of Physics, University of Münster, 48149 Münster, Germany*

Substrate, environment and lattice imperfections have strong impact on the local electronic structure and the optical properties of atomically thin transition metal dichalcogenides. We find by means of scanning tunneling spectroscopy (STS) measurements that the apparent band gap for MoS_2 on SiO_2 is significantly reduced compared to MoS_2 on hBN. Surprisingly, the band gap energies as well as the exciton binding energies determined from all-optical measurements are very similar for MoS_2 on SiO_2 and hBN. This discrepancy is found to be caused by a substantial amount of band tail states near the conduction band edge of MoS_2 supported by SiO_2. The presence of those states impacts the local density of states in STS measurements, manifesting in a broad red-shifted PL peak and a high charge carrier density that is absent using high quality hBN substrates. By accounting for the substrate effects we obtain a quasiparticle gap that is in excellent agreement with optical absorbance spectra and we deduce an exciton binding energy of about $0.53\mathrm{eV}$ on SiO_2 and $0.44\mathrm{eV}$ on hBN.

The electronic structure of atomically thin transition metal dichalcogenides (TMDCs) is unique due to the weak non-local dielectric screening of the Coulomb interaction.[1] The large surface-to-volume ratio makes these materials highly sensitive to changes in the local dielectric environment. This has been exploited as a tuning knob to control excitonic properties and quasiparticle gaps .[2,3] Taking full advantage of TMDCs requires an understanding of the relationship between the electronic and optical properties and their (local) environment. Angle-resolved photo emission spectroscopy, scanning tunneling spectroscopy (STS), photoluminescence excitation spectroscopy and optically probing Rydberg states allow the determination of the quasiparticle band gap $E_{gap}{}^{qp}$ energy.[4–16] The values are typically compared to the onset energy E_{opt} in optical absorbance or photoluminescence spectra to obtain the excitonic binding energy $E_{Bind} = E_{gapqp} - E_{opt}$. Experimental[4,6,7,10–15] and theoretical[3,17–22] values for the binding energy vary widely in the literature, even for similar device geometries. This observation is not fully understood, but local environment is likely to play a key role. TMDC crystals are often prepared by mechanical cleavage and then transferred onto substrates such SiO_2 or hexagonal boron nitride (hBN). It is known that the use of hBN compared to SiO_2 as a substrate significantly enhances the photophysical and electronic properties, greatly reducing inhomogeneous linewidth broadening in photoluminescence (PL) [3,23–26] and enabling large carrier mobilities due to reduced scattering.[27,28] Here, we quantitatively compare STS, optical absorbance and PL spectra recorded on MoS_2 monolayers on SiO_2 and hBN aiming to understand in more detail the underlying mechanisms of the huge differences in the electronic and optical performance of MoS_2 on these two different substrate materials.

Samples are fabricated by mechanical exfoliation and deterministic transfer onto thermally grown SiO_2/Si substrates or few-layer hBN flakes on top of SiO_2/Si. The MoS_2 flakes are contacted by direct transfer onto a thin $30\mathrm{nm}$ Au/$5\mathrm{nm}$ Ti pad or by evaporation of Au/Ti through a shadow mask. STM/STS measurements are taken at room

temperature. The STM is equipped with multiple tips and a scanning electron microscope (SEM) that allows precise location.[29]

Figure 1a shows a false color SEM image of a typical sample. A bias is applied between the biasing (B) and the scanning (S) tip which are both made from PtIr. Additionally, a bias between the tip and the doped Si substrate can be applied to gate the device. A close-up SEM image of a monolayer MoS_2 on hBN and a few-layer MoS_2 sample is shown in Fig. 1b and c. A typical constant current topography map of few-layer MoS_2 is shown in Fig. 1d revealing atomic resolution and the hexagonal lattice symmetry from the topmost sulfur layer. A corresponding line cut is shown in Fig. 1e yielding the expected
S-S distance of 3.17Å.[30]

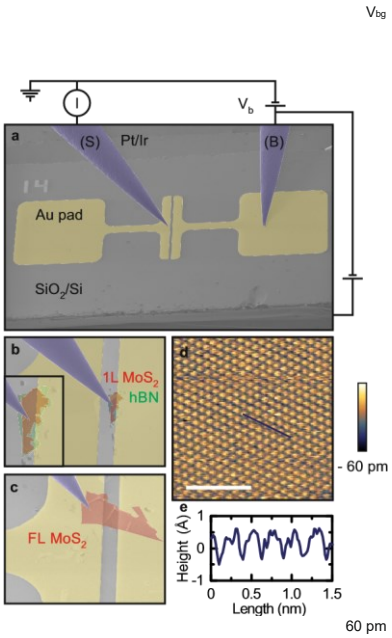

Fig. 1. Room temperature STM of MoS_2. a, SEM image of a gate-tunable sample in the STM chamber. The tunneling current is measured between scanning (S) and biasing (B) tips for a chosen bias voltage V_b. b, Magnified SEM image of a MoS_2 monolayer on top of hBN. c, Magnified SEM image of few-layer MoS_2 on SiO_2. d, Typical constant current STM topography image of a defect-free region from the sample shown in c revealing atomic resolution. e, Corresponding line cut in d showing the interatomic S-S distance.

STS spectra dI/dV that are proportional to the LDOS are shown in Fig. 2a and d for monolayer MoS_2 on hBN and SiO_2, respectively. Vanishing values in the dI/dV spectrum correspond to the absence of electronic states and allow the determination of an apparent gap in the LDOS. For ideal semiconducting materials, the onset of
the dI/dV for negative bias voltages can be assigned to the valence band edge (VB) and the onset for positive bias voltages to the conduction band edge (CB) allowing for the determination of the quasiparticle band gap E_{gap}^{qp}. The position of the Fermi energy is at zero bias voltage. The dI/dV spectrum of monolayer MoS_2 on hBN is shown in Fig. 2a. In order to record the dI/dV curve a backgate voltage of $V_{bg} = 50\text{V}$ is used to reach sufficient in-plane conductivity. The STS measurement shows an apparent gap in the LDOS of $\sim 2.35\text{eV}$ with both the CB and the VB exhibiting a steep increase in density of states. In Fig. 2b, we perform optical absorbance spectroscopy on a nominally identical sample. The spectrum reveals absorption from the A and B exciton transition at 1.89eV and 2.05eV. Converting the absorbance spectrum to the real and imaginary part of the dielectric function utilizing Kramers-Kronig constraint analysis[31] and taking the second derivative[13,32] as shown in Fig. 2c allows us to observe the critical points in the optically active interband transitions that are related to the joint density of states. From this critical point analysis, we determine $E_{gap,Abs}^{qp} \sim 2.33\text{eV}$, which is in excellent agreement with the LDOS gap obtained from STS. Therefore, we assign the LDOS gap from STS to the quasiparticle gap $E_{gap,STS}^{qp} \sim 2.35\,\text{eV}$.
From the emission of the 1s exciton (A exciton), we can directly determine the exciton binding energy through
$E_{Bind} = E_{gapqp} - E_A$. Taking E_{gapqp} from tunneling (absorbance) spectra we obtain an exciton binding energy of $0.46\text{eV}(0.44\text{eV})$ in good agreement with theory that predicts values of $E_{Bind} = 0.3\text{–}0.7\text{eV}$[3,17–20,22] and binding energies obtained from pure optical investigations.[7,13]

The situation is more complex for MoS_2 on the more normally used substrate SiO_2. STS and absorbance spectra as well as the critical point analysis taken on monolayer MoS_2 on SiO_2 are shown in Fig. 2d-f, respectively. Here, MoS_2 on SiO_2 reveals an apparent gap in the LDOS of $\sim 2.1\text{eV}$, a value that is in good agreement with values from STS measurements on monolayer MoS_2 on SiO_2 in literature.[4,6,10–12,14] Intriguingly, we observe the onset of the quasiparticle gap from absorbance measurements in
Fig. 2e,f at an energy of $E_{gap,Abs}^{qp} \sim 2.44\text{eV}$, much higher than the value from the STS data. Determination of the binding energy from pure optical measurements shown in Fig. 2e reveals $E_{Bind} = E_{gap,Abs}^{qp} - E_A = 0.53\text{eV}$, taking into account the lowest optically active interband transition $E_A = 1.91\text{eV}$, in good agreement with theory and other optical

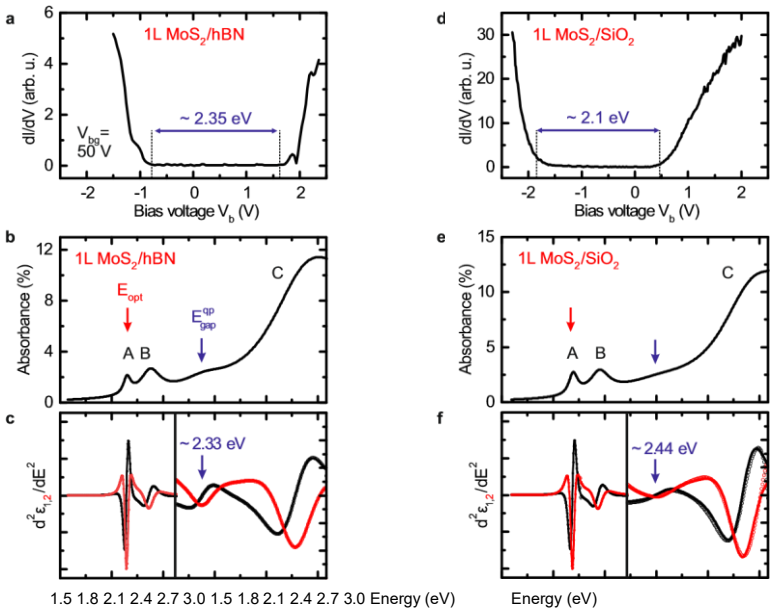

Fig. 2. a, STS spectrum of MoS_2 on hBN taken at $V_{bg} = 50V$. b, Optical absorbance of MoS_2 on hBN. c, Critical point analysis of MoS_2 on hBN. The second derivative of the real (imaginary) part of the dielectric function $\varepsilon_{1(2)}$ are plotted as black (red) traces. Both reveal resonances at the A and B excitonic transitions and a weaker feature at $2.33eV$ associated with $E_{gap}{}^{qp}$. d, STS spectrum of monolayer MoS_2 on SiO_2. e, Optical absorbance of monolayer MoS_2 on SiO_2. f, Critical point analysis of MoS_2 on SiO_2 as in c revealing resonances at the A and B excitonic transitions and a weaker signature at $2.44eV$ associated

measurements, but more than twice the binding energy using the apparent gap from STS measurements shown in Fig. 2d.

In TMDCs, the exciton binding energy directly depends on the surrounding dielectric environment. For the static case and in the limit of long wavelengths ($q \to 0$), the dielectric constant of the environment is approximated by an average dielectric constant from in our case substrate and vacuum [see Supplementary Information (SI) for details].[33] The average dielectric constant is very similar, but slightly larger for MoS_2 on SiO2 ($\varepsilon_{SiO2} = 3.9$.[34]) compared to hBN ($\varepsilon_{hBN} = \sqrt{\varepsilon_{\perp}\varepsilon_{k}} = 5.89$).[35]. We therefore expect an exciton binding energy that is slightly larger for MoS_2 on SiO_2 compared MoS_2 on hBN due to a weaker dielectric screening. This explains why E_{Bind} is very similar on both substrates, but $\sim 90meV$ larger for the MoS_2 on SiO_2 with $E_{bin} \sim 0.44eV$ and $\sim 0.53eV$ for the 1s exciton in MoS_2 on hBN and SiO_2, respectively. From similar considerations, we expect very similar quasiparticle gap energies for MoS_2 on SiO_2 and on hBN in agreement with the optical measurements but in disagreement with the apparent gap in the LDOS from STS.

To investigate the origin of this discrepancy, we directly compare the STS spectra for MoS_2 monolayers on SiO_2 and hBN. We make two main observations: First, it is evident that in addition to the larger STS gap, the Fermi level is shifted close to the middle of the apparent gap in the LDOS with hBN as substrate compared to SiO_2. For MoS_2 on SiO_2, the apparent gap is smaller and the Fermi level is close to the conduction band edge, showing the commonly observed n-type behavior of MoS_2. The origin of excess electrons is not yet fully understood, but has been tentatively attributed with E_{gapqp}.

to defects in the crystal lattice[36] and charge traps in the SiO_2.[25] Second, the rise of LDOS at the conduction band edge is much steeper for monolayers on hBN than on SiO_2 (see Fig. 2a,d). The rise of the LDOS at the valence band edge is similar on both substrates. This is further visualized in Fig. 3a by overlapping the onset for negative bias voltages in the dI/dV traces assigned to the valence band maxima by offsetting the curves to match the spectra taken on both substrates. The STS spectra are almost identical around the VB tail but steepness and onset are significantly different at positive bias voltages assigned to the LDOS at the CB onset. We observe a more slowly rising LDOS with an lower energy onset at the CB for MoS_2 on SiO_2 compared to MoS_2 on hBN. We assign the LDOS at lower energies to the emergence of band tail states (BTS) due to the SiO_2 substrate (see Fig. 3b).[26,37] The surface of SiO_2 is subject to dangling bonds and near-surface charge traps[25] that can severely impact the electronic properties of TMDCs by the introduction of interfacial states.[37] In particular, silanol groups (Si-O-H) are expected at the SiO_2 surface due to O_2 plasma treatment prior to the MoS_2 transfer.[38] The silanol groups are negatively charged and are reported to exist in large densities of

$5{\cdot}10^{14}\mathrm{cm}^{-2}$.[38] Similarly, it has been reported for electronic devices prepared from CVD grown MoS_2 on SiO_2 that the charge transport is severely limited by such band tail states.[39] In the presence of additional states tailing off the CB, the onset of LDOS in STS measurements for positive bias voltages does not directly mark the CB minimum. As a consequence, the onset of the LDOS in STS for MoS_2 on SiO_2 that is often referred to as the CB edge is obscured by the BTS giving the impression of a lowered $E_{gap}{}^{qp}$. Since the emission and absorption energy of the exciton stays unaffected from such BTS, an underestimated exciton binding energy is derived, when using the $E_{gap}{}^{qp}$ from STS measurements as sketched in Fig. 3b.

To visualize the impact of the presence or absence of BTS on the optical interband emission properties, we perform photoluminescence measurements of monolayer MoS_2 on SiO_2, on hBN and for comparison with reports in literature also on fully encapsulated MoS_2 in hBN (see Fig. 3c). To diminish the masking of the emission spectra by thermal broadening, the sample are cooled to $10\mathrm{K}$. The spectra exhibit emission from the neutral exciton X, the negatively charged trion T and the so-called L peak that is attributed to adsorbates and intrinsic defects. Exchanging the SiO_2 with hBN substrate already significantly reduces the free exciton linewidths as recently demonstrated.[3,23,24] The reduced linewidth is accompanied by a significant reduction of the L peak and a slight shift of spectral weight from trion to the neutral exciton indicating less electron doping for. The n-type doping points towards the existence of silanol groups at the SiO_2 substrate that result in unintentional doping of MoS_2. The reduced electron doping for monolayers on hBN contributes to the observation that in STS spectroscopy the Fermi level shifts by almost $1\mathrm{eV}$ closer to the VB as is

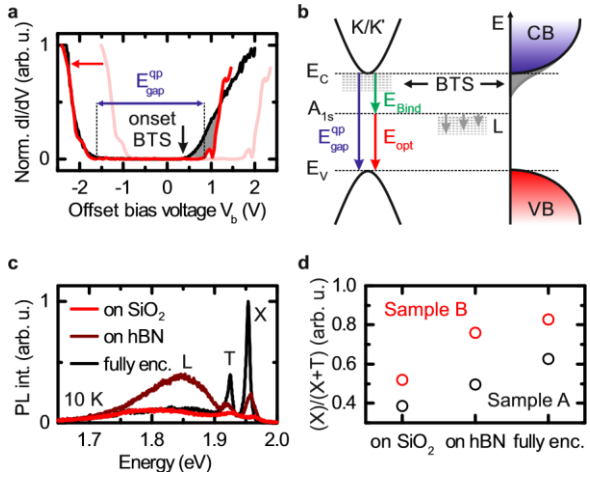

Fig. 3. a, Normalized STS spectra of monolayer MoS_2 on SiO_2 and hBN for direct comparison. Contribution from BTS in the conduction band minimum (CBM) on SiO_2 are highlighted. b, Schematic of the interplay of quasiparticle gap $E_{gap}{}^{qp}$, optical gap E_{opt} and exciton binding energy E_{Bind}. The presence of BTS gives rise to density of electronic states tailing off the conduction band edge. c, Low-temperature ($10\mathrm{K}$) μ-PL of monolayer MoS_2 on SiO_2, on hBN and fully encapsulated between hBN. The spectra show emission from neutral and charged excitons as well as the defect related L-band. d, Spectral weight of the neutral and charged exciton for the corresponding sample geometries in c.

evident in Fig. 2a,d and Fig. 3a. An additional contribution to this large Fermi level shift is expected to be caused by a reduction of the work function of the MoS_2 on hBN compared to MoS_2 on SiO_2, an effect that is widely observed for hBN/metal heterostructures.[40–43] We further quantify the interpretation that the doping is reduced for MoS_2 on hBN by plotting the relative spectral weight of the neutral exciton $\frac{X}{X+T}$ in Fig. 3d for two nominally identical samples. For both samples, we observe that the crystal is more intrinsic when stacked or fully sandwiched in hBN. Moreover, the photoluminescence of the L peak is reduced with respect to the neutral exciton emission for hBN as substrate and further when fully encapsulated.[3,23,24] The origin of L peak emission and intrinsic doping can be manifold but is likely due to a complex interplay of surface adsorbates (physi- and chemisorbed atoms or molecules) and the substrate with the monolayer and its native defects.

Interestingly, for MoS_2 on SiO_2, the energy difference between the onset of the L peak and the neutral exciton X in low-temperature photoluminescence is about $200\mathrm{meV}$ (compare Fig. 3c and schematic in Fig. 3b). This difference is almost identical to the energy difference between the onset of the density of states in STS spectroscopy interpreted as BTS and the actual CB edge as determined from absorbance measurements (see Fig. 2). The similar energy differences suggest that the BTS in STS and the L peak in photoluminescence have the same or very similar origin.

The density of intrinsic defects in the crystal that are predominantly sulfur vacancies as observed in STM topography maps (see SI) is in good agreement with the presence of negatively charged trions in photoluminescence. Here we assume that one excess electron per vacancy results in the intrinsic electron doping of $> 10^{12}\mathrm{cm}^{-2}$ in accordance with literature for MoS_2.[44] Comparing the intrinsic defect density in light of STS measurements, we notice that the hBN apparently passivates the impact of such defects resulting in a reduced electron doping visible by a Fermi energy that is shifted more closely to the center of the band gap in STS, and by a reduced trion and L peak emission in PL measurements. When MoS_2 is interfaced to non-passivated surfaces like SiO_2 or air, atoms and molecules are likely to be physiand chemisorbed to native defects acting e.g. as molecular

gates[44] changing the charge carrier density and the local electronic and optical properties.

To sum up, we interpret intrinsic and extrinsic imperfections to cause the observed BTS, the larger inhomogeneous broadening of excitonic transitions in PL, the L peak emission and intrinsic n-type doping. The BTS appear to be spread over the whole sample and are therefore expected to significantly contribute to charge transport.[26,37] The detrimental influence of extrinsic and intrinsic imperfections can be mitigated by proper choice of the substrate or by fully encapsulating the MoS_2, e.g. in hBN. These results help to understand the influence of substrates and defects on the electronic structure of TMDCs to deterministically tailor their electronic properties.[45]

We acknowledge support of the Deutsche Forschungsgemeinschaft under Germany's Excellence Strategy – EXC 2089/1 – 390776260, EXC-2111 – 390814868, NIM nad projects WU 637/4- 1, HO 3324/9-1, the TUM - IGSSE and ExQM. M.L. was supported by the DFG within RTG 2247 and CPU time at the HLRN (Hannover/Berlin). K.W. and T.T. acknowledge support from the Elemental Strategy Initiativeby the MEXT, Japan and the CREST (JPMJCR15F3), JST. AK and ANP were supported by the NSF MRSEC (DMR-1420634).

10.1103/physrevlett.113.076802.

2 A. Raja, A. Chaves, J. Yu, G. Arefe, H. M. Hill, A. F. Rigosi, T. C. Berkelbach, P. Nagler, C. Schüller, T. Korn, C. Nuckolls, J. Hone, L. M.-H. Chiu, C. Zhang, H.-W. Shiu, C.-P. Chuu, C.-H. Chen, C.-Y. S. Chang, C.-H. Chen, M.-Y. Chou, C.-K. Shih, and L.-J. Li, Nature Communications 6, 7666 (2015).

7 H. M. Hill, A. F. Rigosi, C. Roquelet, A. Chernikov, T. C. Berkelbach, D. R. Reichman, M. S. Hybertsen, L. E. Brus, and T. F. Heinz, Nano Letters 15, 2992 (2015).

8 Y. L. Huang, Y. Chen, W. Zhang, S. Y. Quek, C.-H. Chen, L.-J. Li, W.-T. Hsu, W.-H. Chang, Y. J. Zheng, W. Chen, and A. T. S. Wee, Nature Communications 6, 6298 (2015).

9 R. Addou, L. Colombo, and R. M. Wallace, ACS applied materials & interfaces 7, 11921 (2015).

10 A. F. Rigosi, H. M. Hill, K. T. Rim, G. W. Flynn, and T. F. Heinz, Physical Review B 94, 075440 (2016).

11 X. Zhou, K. Kang, S. Xie, A. Dadgar, N. R. Monahan, X.-Y. Zhu, J. Park, and A. N. Pasupathy, Nano Letters 16, 3148 (2016).

12 H. M. Hill, A. F. Rigosi, K. T. Rim, G. W. Flynn, and T. F. Heinz, Nano Letters 16, 4831 (2016).

13 K. Yao, A. Yan, S. Kahn, A. Suslu, Y. Liang, E. S. Barnard, S. Tongay, A. Zettl, N. J. Borys, and P. J. Schuck, Physical Review letters 119, 087401 (2017).

14 A. Kerelsky, A. Nipane, D. Edelberg, D. Wang, X. Zhou, A. Motmaendadgar, H. Gao, S. Xie, K. Kang, J. Park, J. Teherani, and A. Pasupathy, Nano Letters 17, 5962 (2017). 15

C. Robert, M. A. Semina, F. Cadiz, M. Manca, E. Courtade, T. Taniguchi, K. Watanabe, H. Cai, S. Tongay, B. Lassagne, P. Renucci, T. Amand, X. Marie, M. M. Glazov, and B. Urbaszek, Physical Review

---

* julian.klein@wsi.tum.de

† fmross@mit.edu

‡ wurstbauer@wwu.de

E. Brus, T. F. Heinz, D. R. Reichman, and A. Chernikov, Nature Communications 8, 15251 (2017). 3

M. Florian, M. Hartmann, A. Steinhoff, J. Klein, A. W. Holleitner, J. J. Finley, T. O. Wehling, M. Kaniber, and C. Gies, Nano Letters 18, 2725 (2018).

4 C. Zhang, A. Johnson, C.-L. Hsu, L.-J. Li, and C.-K. Shih, Nano letters 14, 2443 (2014).

5 A. R. Klots, A. K. M. Newaz, B. Wang, D. Prasai, H. Krzyzanowska, J. Lin, D. Caudel, N. J. Ghimire, J. Yan, B. L. Ivanov, K. A. Velizhanin, A. Burger, D. G. Mandrus, N. H. Tolk, S. T. Pantelides, and K. I. Bolotin, Scientific Reports 4, 6608 (2014).

6 A. Chernikov, T. C. Berkelbach, H. M. Hill, A. Rigosi, Y. Li, O. B. Aslan, D. R. Reichman, M. S. Hybertsen, and T. F. Heinz, Physical Review Letters 113 (2014), Materials 2, 011001 (2018). 16 C. Murray, W. Jolie, J. A. Fischer, J. Hall, C. van Efferen, N. Ehlen, A. Grüneis, C. Busse, and T. Michely, Physical Review B 99, 115434 (2019).

17 A. Ramasubramaniam, Physical Review B 86, 115409 (2012). 18

D. Y. Qiu, F. H. da Jornada, and S. G. Louie, Physical Review Letters 111, 216805 (2013).

19 T. Cheiwchanchamnangij and W. R. L. Lambrecht, Physical Review B 85, 205302 (2012).

20 H. Shi, H. Pan, Y.-W. Zhang, and B. I. Yakobson, Physical Review B 87, 155304 (2013).

21 A. Steinhoff, M. Rösner, F. Jahnke, T. O. Wehling, and C. Gies, Nano Letters 14, 3743 (2014).

22

Y. Liang and L. Yang, Physical review letters 114, 063001 (2015).
23 J. Wierzbowski, J. Klein, F. Sigger, C. Straubinger, M. Kremser, T. Taniguchi, K. Watanabe, U. Wurstbauer, A. W. Holleitner, M. Kaniber, K. Müller, and J. J. Finley, Scientific Reports 7 (2017), 10.1038/s41598-017-09739-4.
24 F. Cadiz, E. Courtade, C. Robert, G. Wang, Y. Shen, H. Cai, T. Taniguchi, K. Watanabe, H. Carrere, D. Lagarde, M. Manca, T. Amand, P. Renucci, S. Tongay, X. Marie, and B. Urbaszek, Physical Review X 7, 021026 (2017). 25 K. Dolui, I. Rungger, and S. Sanvito, Physical Review B 87, 165402 (2013).
26 W. Zhu, T. Low, Y.-H. Lee, H. Wang, D. B. Farmer,J. Kong, F. Xia, and P. Avouris, Nature Communications 5, 3087 (2014).
27 X. Cui, G.-H. Lee, Y. D. Kim, G. Arefe, P. Y. Huang, C.-H. Lee, D. A. Chenet, X. Zhang, L. Wang, F. Ye, F. Pizzocchero, B. S. Jessen, K. Watanabe, T. Taniguchi, D. A. Muller, T. Low, P. Kim, and J. Hone, Nature Nanotechnology 10, 534 (2015).
28 C. R. Dean, A. F. Young, I. Meric, C. Lee, L. Wang, S. Sorgenfrei, K. Watanabe, T. Taniguchi, P. Kim, K. L. Shepard, and J. Hone, Nature Nanotechnology 5, 722 (2010).
29 S.-H. Ji, J. B. Hannon, R. M. Tromp, V. Perebeinos, J. Tersoff, and F. M. Ross, Nature Materials 11, 114 (2011).
30 L. F. Mattheiss, Physical Review B 8, 3719 (1973).
31 Y. Li, A. Chernikov, X. Zhang, A. Rigosi, H. M. Hill, A. M. van der Zande, D. A. Chenet, E.-M. Shih, J. Hone, and T. F. Heinz, Physical Review B 90, 205422 (2014).
32 P. Lautenschlager, M. Garriga, L. Vina, and M. Cardona, Phys. Rev. B 36, 4821 (1987).
33 L. V. Keldysh, JETP 29, 658 (1979).
34 H. R. Philipp, Journal of Applied Physics 50, 1053 (1979).
35 R. Geick, C. H. Perry, and G. Rupprecht, Physical Review 146, 543 (1966).
36 J.-Y. Noh, H. Kim, and Y.-S. Kim, Physical Review B 89, 205417 (2014). 37 N. Fang and K. Nagashio, Journal of Physics D: Applied Physics 51, 065110 (2018).
38 K. Nagashio, T. Yamashita, T. Nishimura, K. Kita, and A. Toriumi, Journal of Applied Physics 110, 024513 (2011). 39 W. Zhou, X. Zou, S. Najmaei, Z. Liu, Y. Shi, J. Kong, J. Lou, P. M. Ajayan, B. I. Yakobson, and J.-C. Idrobo, Nano Letters 13, 2615 (2013).
40 M. Morscher, M. Corso, T. Greber, and J. Osterwalder, Surface Science 600, 3280 (2006).
41 F. Schulz, R. Drost, S. K. Hämäläinen, T. Demonchaux, A. P. Seitsonen, and P. Liljeroth, Physical Review B 89, 235429 (2014). 42 Q. Zhang, Y. Chen, C. Zhang, C.-R. Pan, M.-Y. Chou, C. Zeng, and C.-K. Shih, Nature Communications 7, 13843 (2016).
43 Q. Zhang, J. Yu, P. Ebert, C. Zhang, C.-R. Pan, M.-Y. Chou, C.-K. Shih, C. Zeng, and S. Yuan, ACS Nano 12, 9355 (2018). 44 B. Miller, E. Parzinger, A. Vernickel, A. W. Holleitner, and U. Wurstbauer, Applied Physics Letters 106, 122103 (2015). 45 J. Klein, M. Lorke, M. Florian, F. Sigger, L. Sigl, S. Rey, J. Wierzbowski, J. Cerne, K. Müller, E. Mitterreiter, P. Zimmermann, T. Taniguchi, K. Watanabe, U. Wurstbauer, M. Kaniber, M. Knap, R. Schmidt, J. J. Finley, and A. W. Holleitner, Nature Communications 10 (2019), 10.1038/s41467-019-10632-z.